Cellular/Molecular

Thermodynamic Regulation of NKCC1-Mediated Cl^- Cotransport Underlies Plasticity of $GABA_A$ Signaling in Neonatal Neurons

Audrey C. Brumback[1] **and Kevin J. Staley**[2]

[1]Neuroscience Program and Medical Scientist Training Program, University of Colorado Health Sciences Center, Denver, Colorado 80262, and [2]Departments of Neurology and Pediatrics, Massachusetts General Hospital, Boston, Massachusetts 02114

In the adult brain, chloride (Cl^-) influx through $GABA_A$ receptors is an important mechanism of synaptic inhibition. However, under a variety of circumstances, including acquired epilepsy, neuropathic pain, after trains of action potentials or trauma, and during normal early brain development, $GABA_A$ receptor activation excites neurons by gating Cl^- efflux because the intracellular Cl^- concentration (Cl_i) is elevated. These findings require an inducible, active mechanism of chloride accumulation. We used gramicidin-perforated patch recordings to characterize Cl^- transport via NKCC1, the principal neuronal Cl^- accumulator, in neonatal CA1 pyramidal neurons. NKCC1 activity was required to maintain elevated Cl_i such that $GABA_A$ receptor activation was depolarizing. Kinetic analysis of NKCC1 revealed reversible transmembrane Cl^- transport characterized by a large maximum velocity (v_{max}) and high affinity (K_m), so that NKCC1 transport was limited only by the net electrochemical driving force for Na^+, K^+, and Cl^-. At the steady-state Cl_i, NKCC1 was at thermodynamic equilibrium, and there was no evidence of net Cl^- transport. Trains of action potentials that have been previously shown to induce persistent changes in neuronal E_{Cl} (reversal potential for Cl^-) did not alter v_{max} or K_m of NKCC1. Rather, action potentials shifted the thermodynamic set point, the steady-state Cl_i at which there was no net NKCC1-mediated Cl^- transport. The persistent increase in Cl_i required intact $\alpha2/\alpha3$ Na^+-K^+-ATPase activity, indicating that trains of action potentials reset the thermodynamic equilibrium for NKCC1 transport by lowering Na_i. Activity-induced changes in Na^+-K^+-ATPase activity comprise a novel mechanism for persistent alterations in synaptic signaling mediated by GABA.

Key words: **seizure; sodium pump; development; long-term potentiation; dendrite; action potential; gramicidin-perforated patch**

Introduction

Mature neurons are typically hyperpolarized and inhibited by the net chloride (Cl^-) influx mediated by $GABA_A$ receptor activation. In contrast, in the developing brain, GABA depolarizes and excites neurons by gating Cl^- efflux. Whether Cl^- flows into or out of a cell through $GABA_A$ receptor-operated channels depends on the transmembrane Cl^- gradient. Cation chloride cotransporters expressed at different stages of development are thought to regulate intracellular Cl^- concentration (Cl_i), and therefore, the response to GABA (Lu et al., 1999; Marty et al., 2002; Stein et al., 2004; Wang et al., 2005). NKCC1, expressed early in development, transports Na^+, K^+, and Cl^- into the cell in various electroneutral stoichiometries (Geck et al., 1980; Russell, 2000). In the mature brain, KCC2 moves 1 K^+ and 1 Cl^- across the membrane. Normally transport is outward, but transport by KCC2 is reversible and the direction of transport is dictated by the free energy gradients for K^+ and Cl^- (Staley and Proctor, 1999).

In response to a variety of conditions, the polarity of the GABA response can change from hyperpolarizing and inhibitory to depolarizing and excitatory. Examples of such conditions include trauma to postsynaptic (van den Pol et al., 1996) and presynaptic (Coull et al., 2003) neurons, animal models of neuropathic pain (Coull et al., 2003), seizures (Khalilov et al., 2003), and human epilepsy (Cohen et al., 2002). It is clear from developmental studies that reduced expression of NKCC1 (Vardi et al., 2000; Marty et al., 2002; Wang et al., 2002; Ikeda et al., 2003) and increased expression of KCC2 (Clayton et al., 1998; Rivera et al., 1999; Wang et al., 2002) can reverse the polarity of GABA responses.

However, persistent changes in the response to GABA can also occur immediately after trains of action potentials (APs) (Fiumelli et al., 2005). The mechanism by which this rapid and persistent change in the direction of Cl^- flux occurs is not well understood. The purpose of the present work was first to understand the regulation of Cl^- in the developing brain, and then to determine the mechanism by which Cl^- regulation changes after trains of action potentials.

NKCC1-mediated Cl^- transport has been demonstrated and characterized in multiple systems, but not in neonatal neurons, where it contributes to normal development and also to seizure activity (Russell, 2000; Dzhala et al., 2005). Here, we show that NKCC1-mediated Cl^- transport is the principle mechanism by

Received July 25, 2007; revised Nov. 30, 2007; accepted Dec. 1, 2007.

We thank Javier Alvarez-Leefmans for his helpful feedback.

Correspondence should be addressed to Kevin J. Staley, Departments of Neurology and Pediatrics, Massachusetts General Hospital, Boston, MA 02114. E-mail: kstaley@partners.org.

DOI:10.1523/JNEUROSCI.3378-07.2008

 0270-6474/08/281301-12$15.00/0

which neonatal hippocampal pyramidal neurons accumulate Cl_i to make GABA depolarizing. We describe NKCC1 Cl^- cotransport with a model analogous to Ohm's law, in which the combined electrochemical gradients of the transported ions provide the driving force for Cl^- transport and transporter kinetics represent conductance. This thermodynamic model of NKCC1-mediated Cl^- transport is supported by evidence that transport is reversible and the direction is sensitive to changes in intracellular Na^+ and Cl^-. Finally, we show that the $\alpha2/\alpha3$ isoform of Na^+-K^+-ATPase is required for the rapid and persistent increase in Cl_i that occurs after a train of action potentials. Activity-induced changes in Na^+ and K^+ gradients represent a novel form of plasticity in GABAergic signaling.

Materials and Methods

Slice preparation. All animals were housed and cared for according to institutional guidelines. We prepared acute hippocampal slices from male Sprague Dawley rats, age postnatal day 4 (P4) through P6, when NKCC1 expression is high and KCC2 expression is low (Dzhala et al., 2005). The brain was removed and submerged in ice-cold solution containing (in mM) 87 NaCl, 75 sucrose, 2.5 KCl, 25 $NaHCO_3$, 0.5 $CaCl_2 \cdot 2H_2O$, 7 $MgCl_2 \cdot 6H_2O$, 2.25 $NaH_2PO_4 \cdot H_2O$, and 25 glucose. The solution was continuously bubbled with 95% O_2/5% CO_2. The cerebellum was removed with a razor blade, and the brain was cut sagittally into two hemispheres. For each hemisphere, the diencephalon, midbrain, and remaining hindbrain were bluntly dissected away and discarded. Hemispheres were affixed to an agar block (4% agar) attached to the stage of a vibrating blade microtome (Leica Microsystems, Wetzlar, Germany) and submerged in the above ice-cold solution. Horizontal hippocampal slices (400 μm) were cut and placed in a slice chamber at room temperature in a nominally bicarbonate-free incubation solution containing (in mM) 77 NaCl, 73.5 sucrose, 2.5 KCl, 26 HEPES, 1.25 $CaCl_2 \cdot 2H_2O$, 4.5 $MgCl_2 \cdot 6H_2O$, 1.75 $NaH_2PO_4 \cdot H_2O$, and 17.5 glucose. pH was titrated to 7.4 with NaOH. The solution was continuously bubbled with 100% O_2. Slices recovered at room temperature for at least 1 h before experiments.

The $GABA_A$ channel conducts anions, mainly Cl^- and bicarbonate (Bormann et al., 1987). In the present work, we estimate the Cl_i by measuring the reversal potential of GABA-evoked currents (E_{GABA}). E_{GABA} approximates the reversal potential for Cl^- (E_{Cl}) when the bicarbonate flux through the $GABA_A$ channel is minimized. This is achieved by buffering extracellular solutions with HEPES instead of bicarbonate and CO_2 (Staley et al., 1995; Staley and Proctor, 1999). Therefore, in the present work, the incubation solution and artificial CSF (ACSF) in which cells were recorded were buffered with HEPES instead of bicarbonate/CO_2.

Slices were transferred to a submerged slice chamber (Warner Instruments, Hamden, CT) and perfused at 2–3 ml/min at 32°C with nominally CO_2/bicarbonate-free ACSF containing (in mM) 131.5 NaCl, 2.5 KCl, 26 HEPES, 2 $CaCl_2 \cdot 2H_2O$, 2 $MgCl_2 \cdot 6H_2O$, 1.25 $NaH_2PO_4 \cdot H_2O$, 10 glucose, and the $GABA_B$ receptor antagonist CGP 55845A (1 μM). pH was titrated to 7.3 at 32°C with NaOH. The solution was continuously bubbled with 100% O_2. Slices were stabilized with a custom-made harp of platinum wire and nylon strings. CA1 pyramidal neurons were easily visualized with a 40× water-immersion objective using a Zeiss (Thornwood, NY) Axioskop with differential interference contrast optics.

Gramicidin-perforated patch-clamp electrophysiology. Data were collected with a Multiclamp 700A amplifier and digitized at 10 kHz using pClamp 8.2 software (Molecular Devices, Union City, CA). To prevent the Cl^- concentration of the recording electrode from setting the Cl_i, recordings were performed using gramicidin-perforated patch (Abe et al., 1994; Ebihara et al., 1995; Kyrozis and Reichling, 1995). Gramicidin stock (40 mg/ml in DMSO) was prepared daily and diluted to 80 μg/ml in the recording pipette solution containing (in mM) 10 HEPES and 150 KCl ("0 mM $Na_{pipette}$") or 10 HEPES, 141.1 KCl, and 8.9 NaCl ("9 mM $Na_{pipette}$"). pH was titrated to 7.2 with KOH. Osmolarity was titrated to 290 mOsm/L. Recordings used 0 mM $Na_{pipette}$ unless otherwise noted. All cells were recorded with gramicidin-perforated patch except for one. For this single whole-cell recording, the intracellular solution was comprised of (in mM) 121 potassium gluconate, 4 Na_2ATP, 0.3 Na_3GTP, 1 QX-314, 1 EGTA, 10 HEPES, 6 KCl, and 2 $MgCl_2$; pH 7.2 with KOH; 290 mOsm. This solution had 10 mM Cl^- and 8.9 mM Na^+ (same as the 9 mM $Na_{pipette}$ gramicidin recordings). This cell was one of the three cells recorded for the control action potential experiment (see Fig. 6*D*). We included this cell in the data set because it used the same recording pipette Na^+ concentration as the gramicidin-recorded cells, and because the important aspect of this experiment was the change in Cl_i after action potentials, rather than the absolute Cl_i.

Recording pipettes were pulled from nonfilamented thin wall borosilicate glass (Warner Instruments) to resistances of 1.5–5 MΩ. Pipettes were tip-filled with gramicidin-free pipette solution by immersing the tip in gramicidin-free solution while applying negative pressure to the back end of the pipette for 3–5 s. The pipette was then back-filled with gramicidin-containing pipette solution. The gramicidin-free solution at the tip allowed us to apply positive pressure to the electrode without blowing gramicidin solution onto the slice. Pipettes to picospritz GABA were pulled to 3–7 MΩ resistances and back-filled with GABA-containing ACSF.

The recording electrode and GABA puffer pipette were visually guided to the hippocampal CA1 pyramidal cell layer. In current clamp, a gigaohm seal was obtained at the soma. After several minutes, the recording was switched to voltage clamp; the cell was held at or near the measured resting membrane potential. Experiments began once the access resistance fell below 40 MΩ and was stable (usually after 25–60 min). The Cl^- transport kinetics experiments we present here rely on changing Cl_i with an inward or outward Cl^- current. Dendrites have a higher surface-to-volume ratio than the soma, so a Cl^- charge transfer that has almost no effect on somatic Cl_i can significantly change dendritic Cl_i (Staley and Proctor, 1999). Therefore, Cl^- currents were recorded at the soma in response to pressure application of GABA (100 μM in ACSF) to the apical dendrites ~100 μm from the soma (5–15 ms, 5 psi; Picospritzer II, Parker, Fairfield, NJ) (Staley and Proctor, 1999). The optimal location for the GABA puffer pipette was determined by monitoring the size of GABA-evoked currents in the voltage-clamped neuron while advancing the pipette into the slice.

Dendritic currents can be underestimated if the dendrites are inadequately voltage clamped; this is often improved by using Cs^+ in the recording electrode. We chose not to use Cs^+ in these experiments, because we did not want to alter K^+ gradients or NKCC1 transport. To minimize the error, we integrated the GABA-evoked responses over time to obtain the Cl^- charge transfer (Staley and Mody, 1992). Space-clamp error should not affect the accuracy of the estimated Cl^- transport rates because each test current should be affected to the same degree.

Quantification of GABA-evoked currents and calculation of Cl_i. To determine the steady-state E_{Cl}, GABA-evoked currents were recorded during a series of 1 s voltage steps. Nominally bicarbonate-free ACSF was used in all experiments to minimize bicarbonate flux through the GABA channel so that the E_{GABA} would approximate E_{Cl}. Cl^- currents were evoked at five to seven different membrane potentials, in 5 mV increments with the middle step approximately where the currents reversed (E_{Cl}). We usually limited the membrane potential (V_m) range to within ±15 mV of E_{Cl} to minimize the possibility of altering Cl_i with large Cl^- influxes or effluxes. Ten seconds elapsed between each voltage step to prevent receptor desensitization or changes in Cl_i from confounding our results.

We calculated the charge transfer of $GABA_A$ receptor-mediated currents by calculating the integral of the GABA-evoked current waveform after subtracting the baseline current. Charge transfer/voltage plots were obtained by fitting the data to the Goldman–Hodgkin–Katz constant field equation:

$$I = G \times \frac{Cl_o \times V_m F^2}{RT} \times \frac{1 - e^{\frac{F(E_{Cl} - V_m)}{RT}}}{1 - e^{\frac{-V_m F}{RT}}} \quad (1)$$

where I is current; Cl_o is extracellular Cl^- concentration; G = $GABA_A$ channel Cl^- permeability; F is Faraday's constant (96,487 C · mol^{-1});

R is gas constant (8.315 J · mol^{-1} · K^{-1}); and T is temperature (in Kelvins). E_{Cl} is the value of V_m that corresponds to the zero-current condition for the constant field equation (Eq. 1):

$$E_{Cl} = \frac{-RT}{F} \times \ln\left(\frac{Cl_o}{Cl_i}\right). \quad (2)$$

We calculated the Cl_i based on E_{Cl} using Equation 2.

Estimating Cl^- transport. To estimate Cl^- transport, we transiently changed Cl_i and measured the rate at which Cl_i returned to baseline. The experimental protocol is illustrated in Figure 1*B* ("Cl_i depletion") and Figure 2 ("Cl_i load"). To transiently change Cl_i, we created a large driving force for Cl^- to flow into or out of the cell by stepping the V_m to potentials negative (Fig. 1*B*) or positive (Fig. 2) to E_{Cl} for 1 s. Two hundred milliseconds into the voltage step, GABA was puffed onto the apical dendrites. When V_m was hyperpolarized to E_{Cl}, Cl^- efflux through $GABA_A$ channels transiently lowered Cl_i ("Cl_i depletion"). Conversely, when GABA was applied as V_m was depolarized to E_{Cl}, Cl^- influx transiently increased Cl_i ("Cl_i load"). We coupled each Cl_i load or depletion current with a single "test" Cl^- current evoked 1–6 s later. The test current was evoked at a V_m near E_{Cl}, so that small changes in Cl_i caused by the Cl_i load or depletion would be easily seen as a change the direction and/or size of the test current. By measuring the charge transfer of the test currents at 1 s intervals after the Cl_i load or depletion, we estimated the rate at which Cl_i recovered to baseline. We assumed that any voltage-gated currents activated during the voltage steps did not significantly alter our results for two reasons. First, Cl_i consistently returned to baseline within seconds of the Cl_i load or depletion; and second, the test potential had no effect on the time constant of Cl_i recovery.

Cl_i was calculated for each time point by estimating the change in E_{Cl} that would account for the direction and size of each GABA-evoked test current. For the experiments shown in Figure 1 *B–D*, Cl_i was calculated at each time interval according to the steady-state permeability (estimated from the data in Fig. 1*A* and Eq. 1) and the direction and charge transfer of the GABA-evoked Cl^- current at each time interval after Cl_i depletion (Staley and Proctor, 1999). By combining Equations 1 and 2, we estimate Cl_i for each test current:

$$Cl_i = \frac{Cl_o + \dfrac{I \times (I - e^{\frac{-V_m F}{RT}})}{G \times \dfrac{-V_m F^2}{RT}}}{e^{\frac{-V_m F}{RT}}}. \quad (3)$$

Figures 1*D* and 2*C* show Cl_i as a function of seconds after Cl_i depletion. These data were fit with a monoexponential curve (Eq. 4) using a least-squares algorithm where $t = 0$ is the time at which the membrane potential is stepped to a value near E_{Cl} (Fig. 1*B*). We could not use an earlier time point for $t = 0$ because the Cl^- transport measurements would be confounded by the ongoing Cl_i load or depletion current.

$$Cl_i = \Delta Cl_i \times (1 - e^{-t/\tau}) + Cl_{i,t=0} \quad (4)$$

To determine the NKCC1-specific component of Cl_i transport, this protocol was repeated in the same cell after selectively blocking NKCC1 with 10 μM bumetanide (Russell, 2000). In control conditions, Cl_i returns to baseline via NKCC1 and diffusion; in the presence of 10 μM bumetanide, there is only diffusion. To estimate Cl^- transport by NKCC1 alone, we performed a "bumetanide subtraction." In the presence and absence of bumetanide, Cl_i recovered to baseline with monoexponential kinetics (Eq. 4, Fig. 3*B*). Monoexponential rate constants are additive; therefore, the rate constants for NKCC1-mediated Cl^- transport and diffusion were additive:

$$\frac{1}{\tau_{NKCCl}} = \frac{1}{\tau_{control}} - \frac{1}{\tau_{diffusion}}, \quad (5)$$

where $\tau_{control}$ represents the time constant of Cl_i recovery in the absence of bumetanide and $\tau_{diffusion}$ represents the time constant of Cl_i recovery in the presence of 10 μM bumetanide (Fig. 3). Repetitive GABA application can cause $GABA_A$ receptor desensitization. Because receptor desensitization is insensitive to 10 μM bumetanide, it was subtracted out as part of the bumetanide-insensitive change in Cl_i.

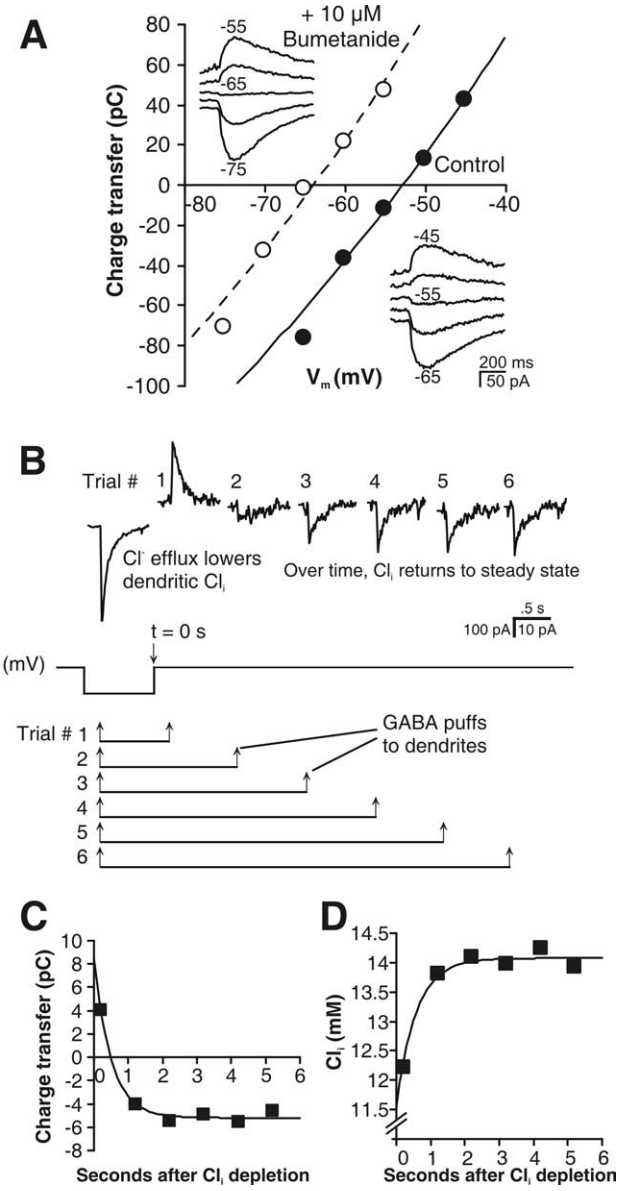

Figure 1. NKCC1 activity is required to maintain elevated Cl_i. In the presence and absence of 10 μM bumetanide, a selective inhibitor of NKCC1, $GABA_A$ receptor-mediated Cl^- conductances were evoked by pressure application of 100 μM GABA to the apical dendrites of a gramicidin-perforated patch-clamped CA1 pyramidal neuron in an acute hippocampal slice from a P5 rat. All cells recorded with 0 mM $Na_{pipette}$. ***A***, Selective NKCC1 inhibition (○) hyperpolarizes E_{Cl} compared with control (●). Fit lines are calculated with the constant field equation (Eq. 1). ***B–D***, "Cl_i depletion": quantification of inward Cl^- transport after dendritic Cl^- efflux lowers Cl_i. ***B***, To lower dendritic Cl_i, V_m was stepped to −123 mV for 1 s, and GABA was applied to the dendrites to elicit a large outward Cl^- flux. V_m was then stepped to −63 mV (3 mV negative to steady-state E_{Cl}), and a second GABA puff evoked a "test" current. Six trials of paired GABA puffs were performed, each with a different delay between Cl_i depletion and the test current. Calibration: 100 pA refers to Cl_i depletion current; 10 pA is for all other currents. ***C***, As the interval between the Cl_i depletion and test current increases, the charge transfer of the test currents returns to steady state. ***D***, Cl_i is calculated from the shift in E_{Cl} that accounts for the direction and charge transfer of each test current. Fit lines in ***C*** and ***D*** are single exponentials (Eq. 4).

Estimating the regulation of Cl^- transport by NKCC1. The rate of Cl^- transport by NKCC1 can be expressed in analogy to Ohm's law:

$$\text{current flow} = \text{driving force} \times \text{conductance}, \quad (6)$$

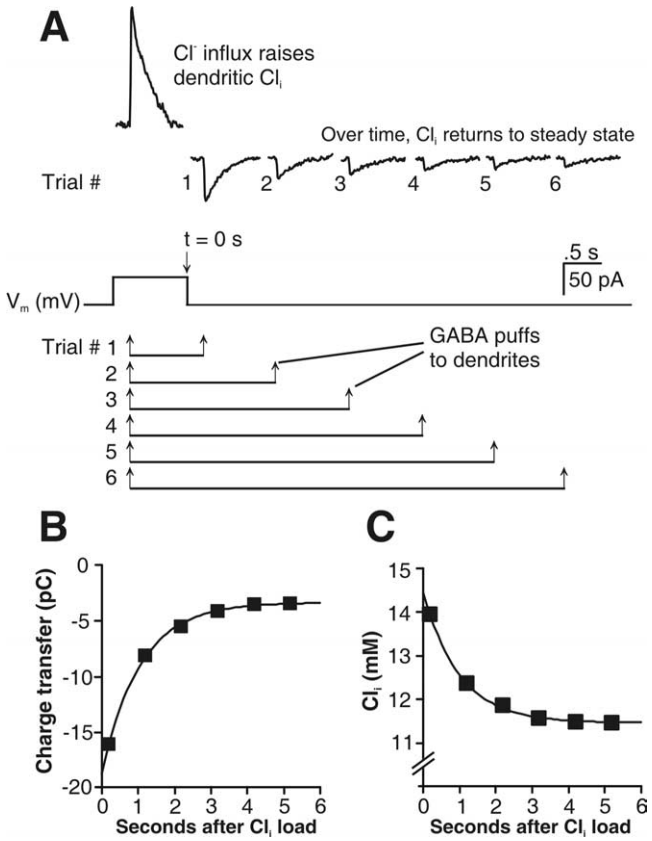

Figure 2. "Cl_i load": quantification of outward Cl^- transport after dendritic Cl^- influx raises Cl_i. The cell was recorded with 9 mM $Na_{pipette}$. ***A***, To raise dendritic Cl_i, V_m was stepped to −5.5 mV for 1 s; 200 ms into the depolarizing voltage step, GABA was applied to the dendrites to elicit a large inward Cl^- flux. V_m was then stepped to −68.5 mV (2.6 mV negative to steady-state E_{Cl}), and a second GABA puff evoked a "test" current. As in Figure 1 *B*, six trials of paired GABA puffs were performed, each with a different delay between Cl_i load and the test current. ***B***, As the interval between the Cl_i load and test current increases, the charge transfer of the test currents returns to steady state. ***C***, Cl_i is calculated from the shift in E_{Cl} that accounts for the direction and charge transfer of each test current. Fit lines in ***B*** and ***C*** are single exponentials (Eq. 4).

where the NKCC1-mediated Cl^- transport rate is analogous to current flow, the combined Na^+, K^+, and Cl^- electrochemical gradient (Eq. 7) produces driving force, and transport capacity (Eq. 9) represents the conductance.

The driving force, or change in free energy (ΔG), associated with NKCC1 Cl^- transport is a function of the transmembrane concentration gradients of the transported ions:

$$\Delta G = \frac{RT}{F}\ln\left(\frac{Na_o^x \times K_o^y \times Cl_o^z}{Na_i^x \times K_i^y \times Cl_i^z}\right), \quad (7)$$

where Na_o, K_o, and Cl_o are the extracellular concentrations and Na_i, K_i, and Cl_i are the intracellular concentration of the transported ions; x:y:z is the ratio of Na^+:K^+:Cl^- transported by NKCC1 (1:1:2, 1:2:3, or 1:4:5). To create a dimensionless term, free energy (driving force) can be normalized to ΔG_{max}, its maximum value at $t = 0$. NKCC1 reaches thermodynamic equilibrium (Cl^- transport rate = 0) when $\Delta G = 0$. The Cl_i at which NKCC1 is at thermodynamic equilibrium ($\Delta G = 0$) is obtained when the bracketed expression in Equation 7 equals 1, or

$$Cl_i = \left(\frac{Na_o^x \times K_o^y \times Cl_o^z}{Na_i^x \times K_i^y}\right)^{\frac{1}{z}}. \quad (8)$$

This equation predicts the Cl_i at which there is no net transport via NKCC1 because there is no net electrochemical driving force to drive transport. The only free variable in the driving force calculation is steady-state Na_i.

The transport capacity (v_{MM}, analogous to the conductance term in Ohm's law) can be modeled using Michaelis–Menten kinetics for enzymatic activity (Läuger, 1987; Alvarez-Leefmans and Russell, 1990; Russell, 2000):

$$v_{mm} = \frac{v_{max} \times [Cl^-]}{K_m + [Cl^-]}, \quad (9)$$

where $[Cl^-]$ is the substrate Cl^- concentration (Cl_o for inward transport; Cl_i for outward transport), v_{max} is the maximum velocity of transport, and K_m is the Cl^- affinity of the transporter (substrate Cl^- concentration at which Cl^- transport is half-maximal). When Cl_i is expressed as a function of seconds after a Cl_i load or depletion, extrapolating the monoexponential fit line (Eq. 4) back to $t = 0$ gives an estimate of v_{max} (the velocity at $t = 0$). Therefore, K_m was the only free variable in calculating transport capacity.

In analogy to Ohm's law (Eq. 6), the velocity of NKCC1-mediated Cl^- transport (v_{NKCC1}) is predicted by multiplying the normalized driving force $\Delta G/\Delta G_{max}$ by the conductance term v_{MM} (Läuger, 1987):

$$v_{NKCCl} = \frac{\Delta G}{\Delta G_{max}} \times v_{MM}. \quad (10)$$

Activity-induced changes in Cl_i. For the experiments presented in Figure 6, neurons were switched from voltage clamp to current clamp; action potentials were evoked by injecting depolarizing current pulses (1.5 ms, 2 nA) at 20 Hz for 2.5 min as described previously (Fiumelli et al., 2005). Recordings were switched back to voltage-clamp mode after the train of action potentials.

Statistical analyses. Student's *t* test was used to test for significant differences between control and experimental conditions. SigmaPlot (SyStat Software, Point Richmond, CA) was used to test whether data were normally distributed. ANOVA with correction for the mean of the observations was used to test the validity of correlations between two variables. In all analyses, $p < 0.05$ was considered significant. All data are presented as mean ± SEM unless noted otherwise.

Drugs. The NKCC1 inhibitor bumetanide was stored as a 50 mM stock solution in ethanol at 4°C (protected from light) and then diluted to 10 μM in ACSF daily. The α2/α3 Na^+-K^+-ATPase inhibitor dihydroouabain (DHO) was diluted directly into ACSF before each experiment. Bumetanide and DHO were bath applied. All chemicals were purchased from Sigma (St. Louis, MO) except QX-314 and CGP 55845A (Tocris, Ellisville, MO).

Junction potentials. Junction potentials were calculated using pClamp 9.2 (Molecular Devices) and subtracted during data analysis: 0 mM $Na_{pipette}$, −3.7 mV; 9 mM $Na_{pipette}$, −3.5 mV; whole cell, −15.2 mV.

Results

NKCC1 is required for depolarizing GABA

The Na^+:K^+:Cl^- transporter NKCC1 is highly expressed in neonatal neurons when GABA is depolarizing and excitatory (Dzhala et al., 2005). To test whether NKCC1 is required for neonatal hippocampal neurons to maintain elevated an elevated Cl_i and therefore depolarize in response to GABA, we measured the resting membrane potential (RMP) and E_{Cl} of voltage-clamped hippocampal CA1 pyramidal cells from postnatal day 4–6 rats. Neurons were recorded in the absence and presence of 10 μM bumetanide, a selective inhibitor of NKCC1 (Gillen et al., 1996; Russell, 2000). We used the gramicidin-perforated patch technique to maintain the native Cl_i. Gramicidin channels are impermeable to anions such as Cl^-, but allow cations (such as Na^+ and K^+) and small uncharged molecules to pass through (Akaike, 1996). The $GABA_A$ channel conducts anions, mainly Cl^- and bicarbonate. To minimize the bicarbonate flux through the $GABA_A$ channel so that $E_{GABA} \approx E_{Cl}$, we used HEPES-buffered (nominally CO_2- and bicarbonate-free) ACSF in all experiments.

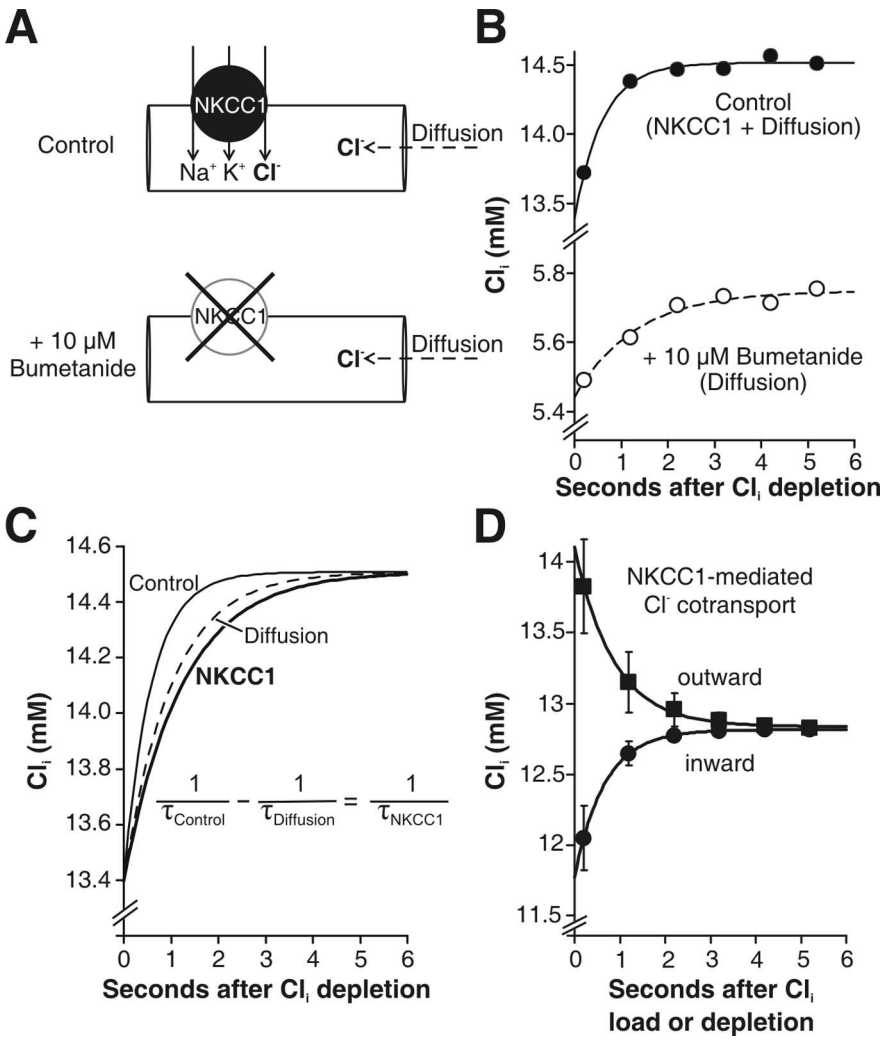

Figure 3. Quantification of NKCC1-mediated Cl^- transport. ***A***, After an acute Cl_i depletion, Cl_i returns to steady state via NKCC1 transport and dendritic diffusion. When NKCC1 is blocked with 10 μM bumetanide, the increase in Cl_i back to steady state is well described by Cl^- diffusion alone (see supplemental material, available at www.jneurosci.org). ***B***, Cl_i as a function of time after Cl_i depletion for control (●) and with NKCC1 blocked (○) for a single neuron recorded with 0 mM $Na_{pipette}$; each is fit by a single exponential. ***C***, The NKCC1 Cl^- transport time constant (τ_{NKCC1}) is determined by subtracting monoexponential rate constants ($k = 1/\tau$). ***D***, After dendritic Cl^- efflux, NKCC1 returns Cl_i to steady state by inward Cl^- transport ($n = 5$, all recorded with 0 mM $Na_{pipette}$). After dendritic Cl^- influx, NKCC1 returns Cl_i to steady state via outward Cl^- transport ($n = 3$, all recorded with 9 mM $Na_{pipette}$). Both inward and outward Cl^- transport recover to the same steady state Cl_i ($p = 0.71$). Inward and outward Cl^- transport data are corrected for non-NKCC1 transport as in ***C*** and are presented as mean ± SEM.

by −37 ± 9% to 8.0 ± 1.5 mM ($n = 5$; $p = 0.02$). Bumetanide had no effect on the $GABA_A$ conductance (control: 20.3 ± 5.7 μS; +Bum: 25.0 ± 6.7 μS; $n = 5$; $p = 0.62$) or holding current (control: −24.7 ± 8.5 pA; +Bum: −31.6 ± 13.8 pA; $n = 6$; $p = 0.47$). All cells were recorded with 0 mM Na^+ in the recording pipette ($Na_{pipette}$). These results indicate that NKCC1 is necessary for neonatal CA1 pyramidal cells to maintain elevated Cl_i and thus enable depolarizing responses to $GABA_A$ receptor activation.

Cl^- transport quantified

NKCC1 is required for neonatal neurons to maintain elevated Cl_i and depolarize in response to GABA. However, NKCC1-mediated Cl^- transport has not been demonstrated or characterized in the developing hippocampus, where it contributes to both normal development and seizures (Dzhala et al., 2005). We measured inward Cl^- transport by transiently lowering Cl_i and monitoring Cl_i at 1 s intervals as it returned to baseline. The experimental protocol is illustrated in Figure 1*B*. First, we measure steady-state (i.e., baseline) E_{Cl}, as in Figure 1*A*. Then, to measure Cl^- transport, we applied a 1 s hyperpolarizing voltage step (usually 60 mV negative to E_{Cl}). Two hundred milliseconds into the voltage step, GABA was puffed onto the apical dendrites. The rationale was that the hyperpolarized V_m created a large driving force for Cl^- efflux; in the small compartment of the dendrite, Cl^- efflux will decrease Cl_i. For the cell in Figure 1*B*, the Cl_i depletion current evokes a Cl^- efflux (shown by the large inward current). V_m was then stepped to a test potential near E_{Cl}, and a second GABA puff was applied. We performed six trials of paired GABA puffs, each trial having a different time interval (range 1–6 s) between the Cl_i depleting current (first GABA puff) and the test current (second GABA puff). Immediately after Cl_i depletion when Cl_i is low, the first test current reflects Cl^- influx. Over a few seconds, as Cl_i increases back to its steady-state level, the test currents reverse and return to baseline. Fifteen seconds elapsed between the each trial. We set $t = 0$ s to be the time at which the hyperpolarizing voltage step ends and V_m is stepped to a potential near E_{Cl}.

Figure 1*A* illustrates the Cl^- currents from a single neuron with the corresponding charge transfer–voltage relationship in the absence and presence of 10 μM bumetanide. V_m was stepped to a test potential for 1 s. Two hundred milliseconds into the voltage step, 100 μM GABA was pressure applied to the apical dendrites ~100 μm from the soma. Cl^- currents were evoked at a new test potential every 10 seconds. At relatively hyperpolarized membrane potentials, the current is inward, which corresponds to Cl^- efflux. At depolarized potentials, GABA evokes outward currents (Cl^- influx). Cl^- charge transfer was calculated as the area under the current curve after baseline subtraction. The charge transfer–voltage relationships and E_{Cl} were calculated with the Goldman–Hodgkin–Katz constant field equation (Eq. 1). On average, Cl^- currents reversed at −64.4 ± 4.4 mV, which corresponds to a Cl_i of 13.1 ± 2.0 mM. Mean RMP was −67.0 ± 1.6 mV. After the addition of 10 μM bumetanide, E_{Cl} hyperpolarized to −77.6 ± 4.5 mV, corresponding to a Cl_i that was lowered

The charge transfer of each test current was calculated by measuring the area under the current waveform after baseline subtraction. Figure 1*C* shows charge transfer as a function of time after Cl_i depletion for the cell illustrated in Figure 1*B*. The first test current is positive, indicating a negative shift in E_{Cl} immediately after Cl_i depletion. Within a few seconds, charge transfer returns to its negative baseline value. To estimate the Cl_i at each time interval, we calculated the change in E_{Cl} that would account for the size and direction of the charge transfer when compared with baseline (please see Materials and Methods for further de-

tails). Figure 1*D* shows that Cl_i rises back to its baseline value within a few seconds after Cl_i depletion for the cell in Figure 1, *B* and *C*.

NKCC1-mediated ion transport is reversible, meaning Cl^- can be transported in or out of the cell (Russell, 2000). We estimated the rate of outward Cl^- transport by calculating Cl_i as a function of time after an increase in Cl_i ("Cl_i load"). Figure 2*A* illustrates the experimental protocol. To measure outward Cl^- transport, we performed a similar experiment to that shown in Figure 1*B–D*. The protocol was the same as in Figure 1*B*, except that V_m was stepped to a depolarizing potential (60 mV positive to E_{Cl}) to provide a large driving force for Cl^- influx to transiently raise Cl_i ("Cl_i load"). Then, at 1 s intervals, we measured the direction and charge transfer of GABA-evoked currents as described above. For the cell in Figure 2, when V_m was depolarized to E_{Cl}, GABA evoked a large outward current (inward Cl^- flux). One second later, GABA evokes a large inward test current, which indicates that the Cl_i load induced a positive shift in E_{Cl}. The size of the test currents decreases back to steady state over the next few seconds. Figure 2*B* shows the charge transfer of the test currents recovering to baseline following the Cl_i load. Figure 2*C* shows the Cl_i at each time interval after the Cl_i load, calculated based on the estimated change in E_{Cl} compared with baseline. After a transient increase, Cl_i decreases back to its steady-state value within several seconds.

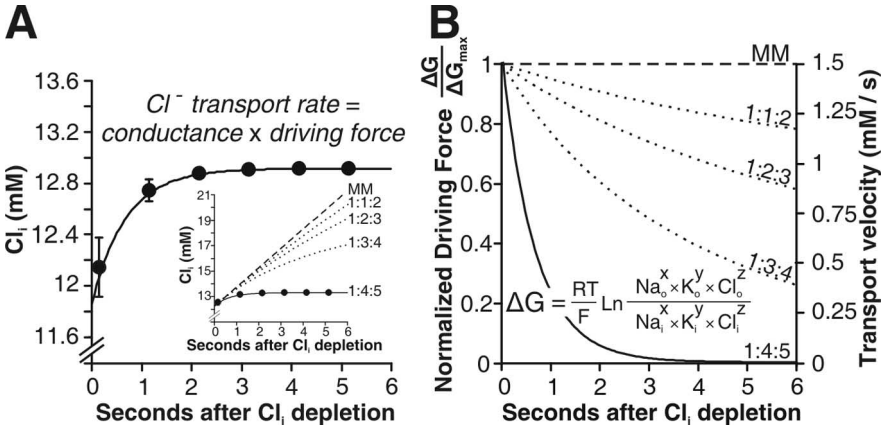

Figure 4. NKCC1 Cl^- transport is thermodynamically regulated and analogous to Ohm's law, current flow = conductance × driving force. ***A***, NKCC1-mediated inward Cl^- transport is best fit by a modified Ohm's law model (Eq. 10) where Cl^- transport velocity (analogous to current flow) equals Michaelis–Menten conductance multiplied by the driving force ($\Delta G/\Delta G_{max}$; ***B***). Data points are the same as presented in Figure 3*D* (●), now fit with the thermodynamic model of transport (1 Na^+:4 K^+:5 Cl^-; Eq. 10) rather than with a simple monoexponential function (Eq. 4). All cells were recorded with 0 mM $Na_{pipette}$. Inset, The driving force depends on the Na^+:K^+:Cl^- transport stoichiometry (1:4:5, solid line). Other ratios (1:1:2, 1:2:3, and 1:3:4; dotted lines) and Michaelis–Menten kinetics alone (dashed line) do not describe NKCC1-mediated Cl^- transport. ***B***, For each transport ratio, the Cl^- transport velocity (right ordinate) parallels the normalized driving force (left ordinate). As Cl_i returns to its steady-state value, the driving force for transport and the velocity of transport go to zero with the same time constant.

NKCC1 Cl^- transport quantified

The techniques described above allow us to measure the rate at which Cl_i returns to baseline after a Cl_i depletion (Fig. 1*B–D*) or load (Fig. 2). In these control conditions, Cl_i most likely returns to steady state by the combination of NKCC1-mediated transport plus non-NKCC1 mechanisms (such as diffusion from neighboring sections of dendrite). This is illustrated in Figure 3*A*. To estimate the NKCC1-specific component of Cl^- transport, we repeated the Cl_i load and depletion experiments in each cell after bath applying 10 μM bumetanide, a selective inhibitor of NKCC1. In the presence of 10 μM bumetanide, Cl_i recovers to baseline by non-NKCC1 mechanisms (Fig. 3*A*). The method used to calculate NKCC1-mediated Cl^- transport is illustrated in Figure 3 and described further in Materials and Methods. Figure 3*B* shows that in control and bumetanide, Cl_i returns to baseline via a monoexponential kinetics (Eq. 4). Monoexponential rate constants ($k = 1/\tau$) are additive, so the rate of NKCC1-specific transport ($1/\tau_{NKCC1}$) was calculated by subtracting non-NKCC1 transport ($1/\tau_{bumetanide}$) from the total ($1/\tau_{control}$). This calculation is shown in Figure 3*C*. Figure 3*D* shows averaged NKCC1-mediated Cl^- transport. After an average decrease in dendritic Cl_i of -1.0 ± 0.3 mM, NKCC1 transports Cl^- into the cell with the time constant (τ_{NKCC1}) of 0.6 ± 0.1 s and a v_{max} of 1.6 ± 0.3 mM/s ($n = 5$; each recorded with 0 mM $Na_{pipette}$). When Cl_i was transiently increased by evoking the first GABA-gated current at a membrane potential positive to E_{Cl}, monoexponential NKCC1-mediated transport kinetics were also demonstrated for outward Cl^- transport when 9 mM Na^+ was included in the perforated patch electrode solution. After an increase in dendritic Cl_i of $+1.3 \pm 0.4$ mM, NKCC1 transported Cl^- out of the cell with $\tau_{NKCC1} = 0.9 \pm 0.3$ s and $v_{max} = 1.6 \pm 0.5$ mM/s ($n = 3$). For both inward and outward Cl^- transport, NKCC1 activity caused Cl_i to relax to the same steady-state value of 12.9 ± 1.3 mM ($n = 8$). NKCC1 transport requires all three transported ions to be present on the side of the membrane from which ions are being transported (Russell, 2000). Consistent with this, no outward NKCC1-mediated Cl^- transport took place in neurons recorded with perforated patch-pipette solution containing 0 mM Na^+ ($\tau_{NKCC1} = 0.1 \pm 2.6$ s; $n = 5$). Data presented in Figures 1, 2, and 3*A–C* are from single cells.

Thermodynamic regulation of NKCC1 and Cl_i

The mechanism by which NKCC1-mediated Cl^- transport sets a particular Cl_i is unknown (Alvarez-Leefmans and Russell, 1990; Russell, 2000). Michaelis–Menten enzyme kinetics models describe the affinity of an enzyme for its substrate (K_m) based on the substrate concentration (Cl_o) and the observed initial/maximum velocity of transport. These models are often used to model Cl^- transport (Michaelis and Menten, 1913; Tas et al., 1987; Gasbjerg and Brahm, 1991; Lauf et al., 1992; Staley and Proctor, 1999). Therefore, we attempted to fit NKCC1-mediated Cl^- transport using Michaelis–Menten kinetic models. Figure 4*A* shows the average data of NKCC1-mediated inward Cl^- transport from Figure 3*D* fit with various transport models. We found that the initial/maximum velocity of Cl^- transport was well described by the Michaelis–Menten model (Eq. 9). However, this model did not fit with the relaxation back to steady-state Cl_i that we observed (Fig. 4*A*, inset), even when the model was modified to include noncompetitive or uncompetitive antagonism by intracellular chloride (data not shown).

Another cation-chloride cotransporter, the neuronal K^+-Cl^- transporter KCC2 (Payne, 1997), is at or near thermodynamic equilibrium at the steady-state K^+ and Cl^- concentrations (Staley and Proctor, 1999). This means that no net transport takes place until a change in the electrochemical gradient of one of the transported ions creates a driving force for ion transport. This is illustrated by the fact that KCC2 Cl^- transport follows a monoexponential relaxation back to the steady-state Cl_i after a Cl_i load or depletion (Staley and Proctor, 1999). We have observed this

same behavior following Cl_i load or depletion with NKCC1-mediated Cl^- transport (Fig. 3*D*). This implies that NKCC1 transport may be thermodynamically regulated as well, meaning that ion transport only takes place when there is an electrochemical driving force to do so (Alvarez-Leefmans and Russell, 1990; Russell, 2000).

We tested the hypothesis that Cl^- transport by NKCC1 is thermodynamically regulated by modeling transport as an analogy to Ohm's law [current = conductance × driving force (Eqs. 6, 10)] (Läuger, 1987). Current represents the rate of NKCC1-mediated Cl^- transport; conductance represents the affinity of the transporter for substrate [calculated by the Michaelis–Menten equation (Eq. 9)], and driving force is provided by the combined electrochemical gradient of the transported ions as a function of the transport ratio (Eq. 7). The only free variables are the steady-state intracellular Na^+ concentration (Na_i) and K_m, NKCC1's affinity for Cl^-, which was consistently high in all experiments (<1 mM). Figure 4*A* shows the NKCC1-mediated Cl^- transport data modeled with various transport ratios. These are the same data points as those shown in Figure 3*D*, now fit with the thermodynamic model (Eq. 10). The data are best described by a thermodynamic model incorporating a transport stoichiometry of 1 Na^+:4 K^+:5 Cl^-. This model predicts thermodynamic equilibrium at a physiologically reasonable Na_i of 3–5 mM (Rose et al., 1999) and steady-state Cl_i equal to the experimentally observed steady state. The inset to Figure 4*A* shows that other transport ratios (1:1:2 and 1:2:3) predict Cl_i to be much higher than the steady-state value we observed. Figure 4*B* shows that the driving force (ΔG) for Cl^- transport and the Cl^- transport velocity are maximal immediately following a Cl_i depletion. As NKCC1 transports Cl^- into the cell, the driving force for transport, and therefore the velocity of transport, decrease to zero as Cl_i returns to steady state. In summary, the results presented thus far show that NKCC1 transports Cl^- in the direction that allows the free energy of the combined Na^+:K^+:Cl^- gradient to return to zero after a transient change in Cl_i.

Our results suggest that NKCC1 transport is regulated by the combined driving force created by the electrochemical gradients of the transported ions. We reasoned that if this were true, changing the transmembrane Na^+ or K^+ gradients should change the driving force for coupled Na^+-K^+-Cl^- transport, and therefore, should change steady-state Cl_i (Eq. 8). Changes in Na_i and K_o would have the most influence on E_{Na} and E_K, and thus the most influence on NKCC1-mediated transport and Cl_i; of the two, Na_i is more labile in single-cell experiments performed in perfused slices. The inward Cl^- transport data presented thus far have been from recordings using 0 mM Na^+ in the recording pipette. To test the hypothesis that altering steady-state Na_i changes steady-state Cl_i, we repeated our gramicidin-perforated patch measurements of NKCC1-mediated inward Cl^- transport using a recording pipette solution containing Na^+ (9 mM $Na_{pipette}$) (Rose and Ransom, 1997). We predicted that compared with recordings with 0 mM $Na_{pipette}$, increased Na_i would decrease steady-state Cl_i by altering the combined electrochemical driving force for NKCC1 transport.

In contrast to our hypothesis, the steady-state Cl_i was not significantly changed (9 mM $Na_{pipette}$: Cl_i = 13.9 ± 1.1 mM; n = 6; 0 mM $Na_{pipette}$: Cl_i = 13.0 ± 1.5 mM; n = 8; p = 0.65). We had assumed that Na_i would equal $Na_{pipette}$, but that is probably not the case. It has been shown that dialysis from the recording pipette solution is progressively less effective at changing ionic equilibria in dendrites because of transmembrane transport along the length of the dendrite (Rose and Ransom, 1997; Yu and Salter, 1998; Jarolimek et al., 1999). Consistent with this, RMP was significantly more negative with 9 mM $Na_{pipette}$ (−74.0 ± 1.2 mV; n = 6) than with 0 mM $Na_{pipette}$ (-66.1 ± 1.5 mV; n = 8; p = 0.002), indicating increased activity of an electrogenic transporter such as Na^+-K^+-ATPase in the cells recorded with 9 mM $Na_{pipette}$ (Jarolimek et al., 1999). Values for Cl_i and RMP here differ slightly from those presented earlier in Results because this data set includes all cells in which we measured Cl_i and RMP, not just those cells in which we measured Cl^- transport kinetics.

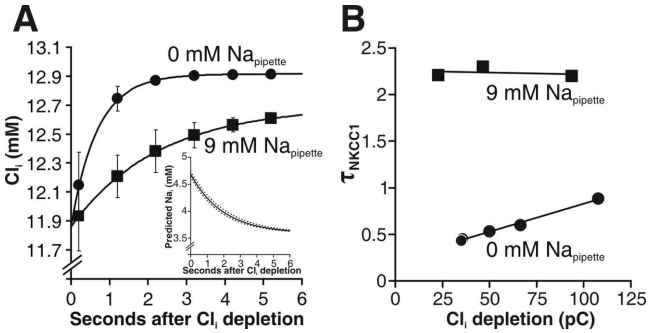

Figure 5. Intracellular sodium thermodynamically limits Cl^- transport by NKCC1. ***A***, NKCC1-mediated Cl^- transport with recording pipette Na^+ concentration ($Na_{pipette}$) of 0 mM (●, n = 5; same data as presented in Figs. 3*D*, 4*A*) or 9 mM (■, n = 3); fit lines were calculated as in Figure 4*A* with a 1 Na^+:4 K^+:5 Cl^- transport ratio (Eq. 10). Inset, The slower initial velocity and τ of NKCC1 Cl^- transport with 9 mM $Na_{pipette}$ can be accounted for by a transient decrease in the free energy available for transport (Fig. 4*B*) arising from a transient increase in Na_i that resolves with a time constant of 1.85 s (solid line). Ninety-five percent confidence interval is shown as dotted lines. ***B***, With 9 mM $Na_{pipette}$, NKCC1 Cl^- transport rate is independent of the size of the Cl_i depletion (■, R^2 = 0.067; n = 3; p = 0.83). With 0 mM $Na_{pipette}$, larger Cl_i depletions correlate with slower NKCC1 Cl^- transport (●, R^2 = 0.99; n = 5; p = 0.0002). Each data point represents NKCC1 transport from one cell. There are two overlapping data points (●) at ~35 pC.

Although the steady-state Cl_i was unaffected by 9 mM $Na_{pipette}$, NKCC1-mediated inward Cl^- transport was significantly slower (τ_{NKCC1} = 2.2 ± 0.03 s; n = 3) than transport with 0 mM $Na_{pipette}$ (τ_{NKCC1} = 0.6 ± 0.1 s; n = 5; p = 0.000006). These data are shown in Figure 5*A*.

The major regulator of Na_i is Na^+-K^+-ATPase. Therefore, Na^+ imported by NKCC1 during coupled Na^+:K^+:Cl^- transport will be cleared from the dendrite via Na^+-K^+-ATPase activity. We hypothesized that the additional 9 mM Na^+ in the recording pipette saturated the cell's Na^+-K^+-ATPase activity, which prevented the Na^+ imported by NKCC1 from being rapidly cleared from the dendrite. We reasoned that the reduced ability to clear imported Na^+ from the dendrite led to a transient Na_i accumulation that reduced the driving force for further NKCC1-mediated transport. According to our thermodynamic model, further Na^+-K^+-Cl^- transport would take place only as quickly as Na^+-K^+-ATPase and diffusion remove the excess Na_i.

To test this hypothesis, we modeled the 9 mM $Na_{pipette}$ Cl^- transport data shown in Figure 5*A* according to a modified version of our thermodynamic model. In previous experiments, Na_i was a free variable with a single steady-state value. To test whether a transient increase in Na_i could account for the difference in Cl^- transport rate between 0 mM $Na_{pipette}$ and 9 mM $Na_{pipette}$, we modified the model to allow Na_i to change over time. We found that the slower transport rate with 9 mM $Na_{pipette}$ was well described when the 0 mM $Na_{pipette}$ Cl^- transport data were combined with a transient increase in Na_i that returns to baseline with a τ of 1.85 s. The predicted Na_i transient is shown in the inset to Figure 5*A*. The transient increase in Na_i that predicts the observed

transport rates is physiologically reasonable, which supports the idea that Na_i and Na^+-K^+-ATPase are important regulators of NKCC1 transport, and therefore, Cl_i.

These results suggest that Na^+ imported by NKCC1 itself can decrease the driving force for further NKCC1 transport if Na^+ is not cleared from the dendrite quickly enough. According to our thermodynamic model, large Cl_i depletions create a large driving force for combined inward Na^+:K^+:Cl^- transport. In the small compartment of the dendrite, a large Cl_i depletion could therefore increase Na_i to the extent that further inward NKCC1 transport is inhibited.

To test the hypothesis that large Cl_i depletions correlate with slow transport, we examined the relationship between τ_{NKCC1} and the size of the Cl_i depletion in recordings made with 0 or 9 mM Na^+ in the recording pipette ($Na_{pipette}$). These data are shown in Figure 5*B*. In recordings with 0 mM $Na_{pipette}$, reduced NKCC1 transport rate (increased τ_{NKCC1}) correlated with increased size of the Cl_i depletion ($R^2 = 0.99$; $n = 5$; $p = 0.0002$). This suggests that transient increases in Na_i by NKCC1-mediated Na^+:K^+:Cl^- transport limit the velocity of further NKCC1 transport. In contrast, no relationship between Cl_i depletion size and NKCC1 transport rate was seen in recordings with 9 mM $Na_{pipette}$ ($R^2 = 0.067$; $n = 3$; $p = 0.83$). This is consistent with Na^+ export (presumably by Na^+-K^+-ATPase) that was already saturated by the combination of pipette Na^+ and the NKCC1-mediated Na^+ influx triggered by even the smallest of Cl_i depletions. Together, these results support the thermodynamic model of NKCC1 Cl^- transport and provide further evidence that Na_i is a key regulator of NKCC1, and therefore, Cl_i.

Action potentials increase steady-state Cl_i and improve Na^+ handling

Thus far, we have examined the thermodynamic regulation of NKCC1 transport, the major Cl_i accumulation mechanism in neonatal neurons. Our thermodynamic model of Cl^- transport provides the tools to test specific hypotheses about activity-dependent changes in Cl_i. Consider the following: trains of action potentials have been shown to cause persistent increases in neuronal Cl_i (Woodin et al., 2003; Fiumelli et al., 2005). Trains of action potentials are also known to cause long-lasting increases in Na^+-K^+-ATPase activity, which lowers Na_i (Ritchie and Straub, 1957; McDougal and Osborn, 1976; Thompson and Prince, 1986; Morita et al., 1993; Parker et al., 1996). The results we have presented thus far have shown that NKCC1 transport is thermodynamically regulated and sensitive to changes in Na_i. If Na_i can limit inward Cl^- transport as our data suggest, then Na^+-K^+-ATPase activity, which sets Na_i, must be integral to controlling the concentration of Cl^- in the cell. Because trains of action potentials increase Na^+-K^+-ATPase activity, the changes in Cl_i observed following action potential trains could be caused by altered Na^+ and K^+ transmembrane gradients from increased Na^+-K^+-ATPase activity. A decreased steady-state Na_i would shift NKCC1's thermodynamic equilibrium such that net Cl^- transport would come to rest at a higher steady-state Cl_i (Eq. 8; see Fig. 7).

We hypothesized that if NKCC1-mediated transport is thermodynamically limited, as our results suggest, changes in the Na^+ and K^+ gradients mediated by increased Na^+-K^+-ATPase activity should result in persistent changes in Cl_i. To test this hypothesis, steady-state E_{Cl} and Cl^- transport kinetics were measured before and after a 20 Hz, 2.5 min train of action potentials in the recorded cell (Fiumelli et al., 2005). Data from a representative cell are shown in Figure 6, *A* and *B*. The action potential

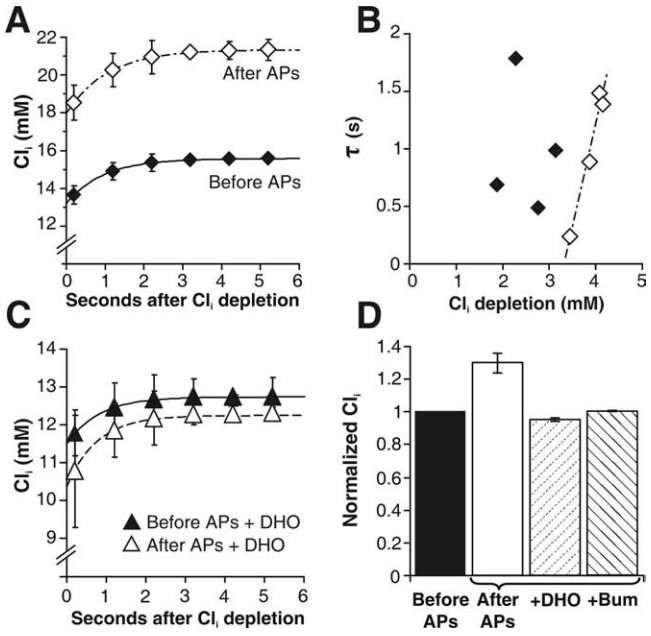

Figure 6. Activity-dependent, long-term increases in Cl_i require Na^+-K^+-ATPase and NKCC1. All cells recorded with 9 mM $Na_{pipette}$. ***A***, After a train of action potentials in the recorded cell (20 Hz, 2.5 min) (Fiumelli et al., 2005), Cl_i reaches a persistently higher steady state. Data from a single cell are shown as mean ± SD. ***B***, Cl^- transport rate as a function of the magnitude of Cl^- depletion before (♦) and after postsynaptic action potentials (◇) for the cell in ***A***. As in Figure 5*B*, in control conditions, there is no relationship between the size of the Cl_i depletion and Cl^- transport rate. After the train of action potentials, Cl^- transport with 9 mM $Na_{pipette}$ more closely resembles Cl^- transport with 0 mM $Na_{pipette}$ (Fig. 5*B*) in that larger Cl_i depletions correlate with slower NKCC1 Cl^- transport. ***C***, The selective $\alpha2/\alpha3$ Na^+-K^+-ATPase antagonist DHO (10 μM) prevents the persistent increase in Cl_i after the train of action potentials. Data from a single cell are presented as mean ± SD. ***D***, Inhibition of $\alpha2/\alpha3$ Na^+-K^+-ATPase ($n = 4$) or NKCC1 ($n = 2$) prevents the persistent increase in Cl_i after a train of action potentials. For each cell, Cl_i was normalized to its value before action potentials.

train caused a persistent increase in Cl_i of 3.7 ± 0.5 mM following the action potentials (Cl_i before APs, 13.6 ± 3.1 mM; Cl_i after APs, 17.3 ± 3.4 mM; $n = 3$; $p = 0.02$). Based on steady-state Cl_i, the calculated steady-state Na_i decreased from 2.7 mM before APs to 0.8 mM after APs for NKCC1 at thermodynamic equilibrium (Eq. 8). We monitored Cl_i in these cells for 27, 33, and 42 min following the train of action potentials. Therefore, in reference to these results, "persistent" means up to 42 min after action potentials. There was no change in holding current during that time (before APs: −22 ± 15 pA; after APs: −23 ± 13 pA; $n = 3$; $p = 0.69$). In control conditions, as in previous experiments with 9 mM Na^+ in the patch pipette (Fig. 5*B*), there was no correlation between the Cl^- transport rate and the size of the Cl_i depletion ($R^2 = 0.02$; $p = 0.87$). However, in the same cells after the train of action potentials, slower Cl^- transport correlated with larger Cl_i transients, as it had in previous experiments with 0 mM Na^+ in the recording pipette. ($R^2 = 0.97$; $p = 0.02$). In other words, action potentials caused Cl^- transport in neurons recorded with 9 mM $Na_{pipette}$ to behave as if they were being recorded with 0 mM $Na_{pipette}$ (compare with Fig. 5*B*). These results imply that in control conditions, the Na^+ load from the recording pipette had saturated the mechanisms by which Na^+ is cleared from the dendrite. Therefore, the Na^+ imported by NKCC1 after even the smallest Cl_i depletion was sufficient to slow down further inward Cl^- transport. In contrast, after the action potentials, larger Cl_i depletions correlated with slower Cl^- transport (as we saw in recordings with 0 mM $Na_{pipette}$). This implies a persistently lower

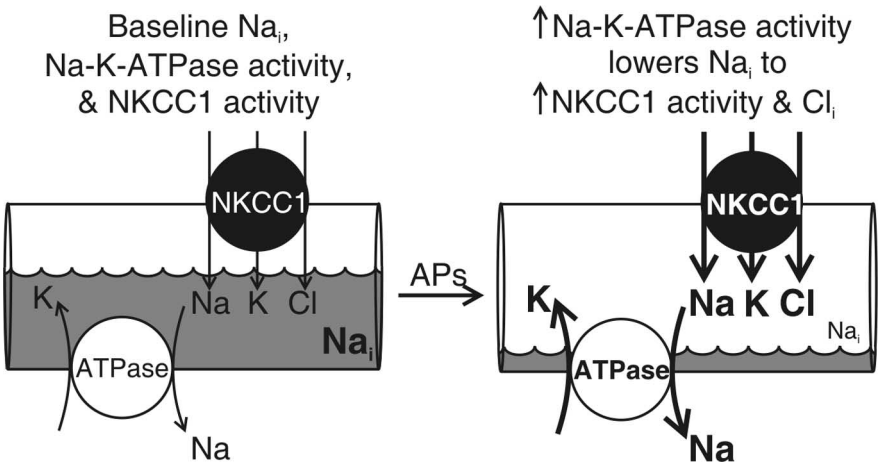

Figure 7. Action potentials increase Cl_i by increasing Na^+ export by Na^+-K^+-ATPase. Left, In control conditions, Na^+-K^+-ATPase activity determines the baseline Na_i (gray liquid), which determines the rate of NKCC1 transport and therefore, Cl_i. Right, After a train of action potentials, increased $\alpha2/\alpha3$ Na^+-K^+-ATPase activity leads to a decrease in Na_i. Low steady-state Na_i increases steady-state Cl_i by shifting the driving force for NKCC1-mediated Cl^- transport (Eq. 8).

Na_i and/or an improved ability to rapidly clear Na^+ from the dendrite. Either mechanism could be explained by an increase in Na^+-K^+-ATPase activity (Fig. 7).

$\alpha2/\alpha3$ Na^+-K^+-ATPase is required for activity-induced increase in Cl_i

We proposed that an activity-dependent increase in Na^+-K^+-ATPase activity was responsible for altering Na_i and thus the Cl_i at which NKCC1 comes to electrochemical equilibrium. We reasoned that if this were true, then blocking Na^+-K^+-ATPase should prevent the persistent increase in Cl_i observed following trains of action potentials. We hypothesized that the "auxiliary" $\alpha2$ and/or $\alpha3$ Na^+-K^+-ATPase isoforms were responsible for the activity-induced change in Na^+ handling by the cell and the change in Cl^- transport. To test this hypothesis, we bath applied the selective $\alpha2/\alpha3$ Na^+-K^+-ATPase inhibitor DHO (10 μM), and then measured steady-state E_{Cl} and Cl^- transport kinetics before and after a 20 Hz, 2.5 min train of action potentials in the recorded cell. Representative data are illustrated in Figure 6*C*.

In control conditions, DHO had no effect on Cl_i compared with control cells (control: 13.6 ± 3.1 mM; $n = 3$; DHO: 15.4 ± 3.1 mM; $n = 4$; $p = 0.71$). However, in the presence of DHO, action potential trains decreased steady-state Cl_i by 0.9 ± 0.02 mM ($n = 4$; $p = 0.01$), corresponding to an increase in Na_i of ~0.6 mM (Eq. 8). These results contrast with those from previous experiments performed without DHO in which action potentials increased Cl_i with a corresponding decrease in Na_i. This implies that without functional $\alpha2/\alpha3$ Na^+-K^+-ATPase, the Na^+ imported into the dendrite during the action potentials increased Na_i to the point that the thermodynamic equilibrium for NKCC1 reset to a lower steady-state Cl_i (Fig. 7). Furthermore, in the presence of DHO, there was no relationship between the time constant of Cl^- transport (τ) and the size of the Cl_i depletion, neither before nor after the train of action potentials [for the cell in Fig. 6*C*, τ versus Cl_i depletion (pC): +DHO before APs: $R^2 = 0.36 \pm 0.97$; $p = 0.59$; +DHO after APs: $R^2 = 0 \pm 0.68$; $p = 0.99$]. In other words, selectively blocking the $\alpha2/\alpha3$ Na^+-K^+-ATPase with DHO prevented the train of action potentials from making transport with 9 mM $Na_{pipette}$ more closely resemble transport with 0 mM $Na_{pipette}$. These results were in direct contrast to previous experiments showing that with intact $\alpha2/\alpha3$ Na^+-K^+-ATPase activity, the train action potentials induced a direct relationship between the rate of Cl^- transport and the size of the Cl_i depletion (Fig. 6*B*). These results indicate that $\alpha2/\alpha3$ Na^+-K^+-ATPase isoforms are required for trains of action potentials to bring about persistent increases in the steady-state Cl_i. These data also support the conclusion that NKCC1-mediated Cl^- transport is controlled by the combined electrochemical gradient of the transported ions such that Cl_i is sensitive to changes in Na_i.

After the addition of DHO, there were no significant changes in holding current (control: −8.5 ± 6.1 pA; +DHO: −7.2 ± 7.7 pA; $n = 4$; $p = 0.59$), input resistance (control: 159.7 ± 104.3 MΩ; +DHO: 204.8 ± 134.9 MΩ; $n = 4$; $p = 0.24$), or resting membrane potential (control: −64.0 ± 2.4 mV; +DHO: −63.9 ± 2.7 mV; $n = 4$; $p = 0.90$), implying that the $\alpha2/\alpha3$ isoforms do not significantly contribute to the cell's baseline functioning. Furthermore, DHO did not change action potential peak amplitude (control: 99.8 ± 0.01 mV; +DHO: 99.8 ± 0.01 mV; $n = 4$; $p = 0.44$) or half-width (control: 4.9 ± 1.1 ms; +DHO: 4.7 ± 0.2 ms; $n = 4$; $p = 0.83$), indicating that the lack of activity-dependent changes in the presence of DHO was not an artifact of defective action potential firing.

Finally, we tested the hypothesis that NKCC1 was necessary for the activity-induced increase in Cl_i. When NKCC1 was inhibited by 10 μM bumetanide, action potential trains had no effect on Cl_i ($n = 2$) (Fiumelli et al., 2005). Together, these results indicate that an activity-dependent increase in Na^+-K^+-ATPase activity alters the transmembrane gradients of Na^+ and K^+ such that a new equilibrium point is reached for NKCC1-mediated Cl^- transport.

Discussion

In the present work, we show that neonatal rat CA1 pyramidal neurons require NKCC1 activity to maintain elevated Cl_i to the extent that GABA is depolarizing. When NKCC1 is selectively blocked with 10 μM bumetanide, the resting Cl_i drops by more than one-third to make GABA inhibitory. We show that after a transient decrease in Cl_i, NKCC1 transports Cl^- into the cell, and after an increase in Cl_i, NKCC1 transports Cl^- out of the cell. This is best explained by equilibrative transport: transient changes in Cl_i create a driving force for coupled Na^+:K^+:Cl^- transport that diminishes to zero as Cl_i returns to steady state. In neonatal hippocampal pyramidal neurons, NKCC1 transport is thermodynamically regulated by the combined Na^+, K^+, and Cl^- electrochemical gradients and is consistent with a net Na^+:K^+:Cl^- transport ratio of 1:4:5.

We investigated activity-dependent changes in E_{Cl} and found that trains of action potentials persistently increased the steady-state Cl_i and made Cl^- transport with 9 mM $Na_{pipette}$ more closely resemble transport with 0 mM $Na_{pipette}$ (Fig. 7). Three Na^+-K^+-ATPase isoforms have been described in neurons. The $\alpha1$ is uniformly expressed on the plasma membrane, whereas the $\alpha2$ and $\alpha3$ isoforms are expressed in a pattern on the plasma membrane that parallels the underlying endoplasmic reticulum (Juhaszova and Blaustein, 1997). The $\alpha1$ isoform is thought to control the bulk intracellular Na^+ concentration; the $\alpha2$ and $\alpha3$ subunits are

considered "auxiliary" isoforms that are recruited during increased cellular activity (Blanco and Mercer, 1998). The α1 isoform has a low affinity for ouabain and is therefore unaffected by 10 μM DHO (McCarren and Alger, 1987; Sweadner, 1989; Berrebi-Bertrand et al., 1990), whereas the α2/α3 isoforms are relatively ouabain sensitive and selectively inhibited by 10 μM DHO (Gao et al., 1995; Juhaszova and Blaustein, 1997). Dihydroouabain prevented the activity-induced changes in Cl_i and the saturating Na^+ condition for NKCC1 transport, indicating that α2/α3 isoforms of Na^+-K^+-ATPase were necessary for the activity-dependent increase in Cl_i. Plasticity of Na^+-K^+-ATPase activity is well established (Therien and Blostein, 2000), and is a logical means of altering neuronal signaling (Ross and Soltesz, 2001), but this is the first demonstration of involvement of Na^+-K^+-ATPase or NKCC1 in long-term synaptic plasticity.

This is also the first quantification of NKCC1-mediated Cl^- transport in the neonatal hippocampus. Our results confirm and extend previous reports on the kinetics of NKCC1 transport in a variety of experimental systems (Russell, 2000). A benefit of the electrophysiology technique is that we observed NKCC1 Cl^- transport with the time resolution of seconds, rather than minutes. Most estimates of NKCC1 transport rates come from measurement of bumetanide-sensitive ^{86}Rb flux (Rb^+ substitutes for K^+). Reported transport rates are on the order of pmol · cm^{-2} · s^{-1}. One pmol · cm^{-2} · s^{-1} corresponds to ~14 mM/s in a dendrite of the geometry calculated in supplemental material (available at www.jneurosci.org). These rates of transport are compatible with the rates we observed, given the differences in the time resolution of the techniques, the levels of NKCC1 expression, and the ion gradients at which transport was measured. Our results are also consistent with the change in Cl^- transport as a function of developmental age and level of synaptic activity (Ben Ari, 2002; Achilles et al., 2007).

The RMP measurements we report here are slightly depolarized compared with the gramicidin-perforated patch measurements by Tyzio et al. (2003). This could be attributable to the differences between CA3 and CA1 neurons or a difference between Wistar and Sprague Dawley rats, because it has been shown that Long–Evans and Sprague Dawley rats are 2 d off from each other developmentally (Talos et al., 2006). In the absence of NKCC1 (if there are no other mechanisms to change Cl_i), Cl^- will be passively distributed (E_{Cl} = RMP). Here, we show that E_{Cl} is 10 mV negative to RMP in the absence of NKCC1 activity. It has been shown in neonatal CA3 pyramidal neurons that the RMP measured with gramicidin-perforated patch is depolarized compared with RMP measured with noninvasive cell-attached techniques (Tyzio et al., 2003). Tyzio et al. (2003) reported that in cell-attached recordings of CA3 pyramidal cells RMP was stable at −77 mV throughout development, which is the value we report here for E_{Cl} in the absence of NKCC1 activity. It is possible that gramicidin recordings distort RMP locally (at the soma), with less distortion in dendrites, such that the dendritic RMP was more negative than our measured somatic RMP (Tyzio et al., 2003).

KCC2 mediates mostly outward Cl^- transport in mature neurons; low levels of expression in this age group could account for the hyperpolarized E_{Cl} in the absence of NKCC1 activity (Dzhala et al., 2005). The kinetics we describe for NKCC1 are similar to those reported for KCC2 (Staley and Proctor, 1999). Both transporters have maximum transport rates in the range of mmol · L^{-1} · s^{-1}, which has important implications for a "push–pull" model of Cl^- homeostasis, where the two transporters could work in concert to maintain steady-state Cl_i. This hypothesis of coupled inward and outward Cl^- transport is attractive from the point of view of precise Cl_i control. However, oppositely directed transporters operating at these velocities would waste enormous amounts of ATP so that Na^+-K^+-ATPase could maintain the necessary transmembrane ion gradients. We have applied 100 μM bumetanide, a concentration that inhibits KCC2, at the end of some experiments (data not shown), and have not observed any change in Cl_i beyond what was seen with 10 μM bumetanide, suggesting that KCC2 does not contribute significantly to Cl_i in the neonatal period.

Action potentials caused a persistent increase in Cl_i that required intact α2/α3 Na^+-K^+-ATPase activity. It has been shown that the increase in Na^+-K^+-ATPase activity that occurs following neuronal activity is transient (Thompson and Prince, 1986). Consistent with this, there was no change in holding current up to 42 min following the train of action potentials, suggesting that Na^+-K^+-ATPase activity was not persistently increased. This implies that once a new lower steady-state Na_i has been reached, the Na^+ pump does not need to continue running at an increased rate to maintain the lower steady-state Na_i. However, we cannot exclude a longer-lasting change in α2/α3 Na^+-K^+-ATPase activity because once Na_i is low, the pump current may be so small that it does not make a significant contribution to the resting membrane potential and holding current.

Inducible modifications of E_{GABA} mediated by activity-dependent alterations in Na^+-K^+-ATPase activity represents a fundamental new motif of long-term synaptic plasticity. There are undoubtedly many mechanisms underlying long-term plasticity of GABA signaling as a result of persistent changes in E_{GABA}, and these mechanisms are likely to vary depending on the age and conditions under which plasticity is studied (van den Pol et al., 1996; Cohen et al., 2002; Coull et al., 2003, 2005; Khalilov et al., 2003; Woodin et al., 2003; Fiumelli et al., 2005). For example, changes in NKCC1 and KCC2 phosphorylation (Kahle et al., 2005) and membrane trafficking (Del Castillo et al., 2005) as well as changes in KCC2 activity have been demonstrated to be important under appropriate conditions (De Koninck, 2007). Here we establish an entirely new mechanism: activity-dependent long-term changes in E_{GABA} in the developing nervous system can be caused by activity-dependent changes in Na^+-K^+-ATPase activity (McDougal and Osborn, 1976; Thompson and Prince, 1986; Ross and Soltesz, 2001), which alter the Cl_i at which a secondary active Cl^- transporter is at equilibrium (Fig. 7). Our findings emphasize the variety of mechanisms that may contribute to plasticity of E_{GABA} and the caution that should be used in extrapolating such mechanisms from one experimental condition to another. With these cautions in mind, our findings may be relevant to the correlated circadian fluctuations in E_{Cl} and Na^+-K^+-ATPase activity observed in hypothalamic suprachiasmatic nucleus neurons (Wagner et al., 1997; Wang and Huang, 2004). Finally, the finding that NKCC1 is at thermodynamic equilibrium at the steady-state Cl_i in neurons suggests caution in the interpretation of E_{GABA} determined by gramicidin-perforated patch recordings, because these recordings may indirectly alter E_{Cl} by altering Na^+ and K^+ gradients.

References

Abe Y, Furukawa K, Itoyama Y, Akaike N (1994) Glycine response in acutely dissociated ventromedial hypothalamic neuron of the rat: new approach with gramicidin perforated patch-clamp technique. J Neurophysiol 72:1530–1537.

Achilles K, Okabe A, Ikeda M, Shimizu-Okabe C, Yamada J, Fukuda A, Luhmann HJ, Kilb W (2007) Kinetic properties of Cl uptake mediated by

Na^+-dependent K^+-2Cl cotransport in immature rat neocortical neurons. J Neurosci 27:8616–8627.

Akaike N (1996) Gramicidin perforated patch recording and intracellular chloride activity in excitable cells. Prog Biophys Mol Biol 65:251–264.

Alvarez-Leefmans FJ, Russell JM (1990) Chloride channels and carriers in nerve, muscle, and glial cells. New York: Plenum.

Ben Ari Y (2002) Excitatory actions of GABA during development: the nature of the nurture. Nat Rev Neurosci 3:728–739.

Berrebi-Bertrand I, Maixent JM, Christe G, Lelievre LG (1990) Two active Na^+/K^+-ATPases of high affinity for ouabain in adult rat brain membranes. Biochim Biophys Acta 1021:148–156.

Blanco G, Mercer RW (1998) Isozymes of the Na-K-ATPase: heterogeneity in structure, diversity in function. Am J Physiol 275:F633–F650.

Bormann J, Hamill OP, Sakmann B (1987) Mechanism of anion permeation through channels gated by glycine and gamma-aminobutyric acid in mouse cultured spinal neurones. J Physiol (Lond) 385:243–286.

Clayton GH, Owens GC, Wolff JS, Smith RL (1998) Ontogeny of cation-Cl^- cotransporter expression in rat neocortex. Brain Res Dev Brain Res 109:281–292.

Cohen I, Navarro V, Clemenceau S, Baulac M, Miles R (2002) On the origin of interictal activity in human temporal lobe epilepsy in vitro. Science 298:1418–1421.

Coull JA, Boudreau D, Bachand K, Prescott SA, Nault F, Sik A, De Koninck P, De Koninck Y (2003) Trans-synaptic shift in anion gradient in spinal lamina I neurons as a mechanism of neuropathic pain. Nature 424:938–942.

Coull JAM, Beggs S, Boudreau D, Boivin D, Tsuda M, Inoue K, Gravel C, Salter MW, De Koninck Y (2005) BDNF from microglia causes the shift in neuronal anion gradient underlying neuropathic pain. Nature 438:1017–1021.

De Koninck Y (2007) Altered chloride homeostasis in neurological disorders: a new target. Curr Opin Pharmacol 7:93–99.

Del Castillo IC, Fedor-Chaiken M, Song JC, Starlinger V, Yoo J, Matlin KS, Matthews JB (2005) Dynamic regulation of Na^+-K^+-2Cl^- cotransporter surface expression by PKC-ε in Cl^--secretory epithelia. Am J Physiol Cell Physiol 289:C1332–C1342.

Dzhala VI, Talos DM, Sdrulla DA, Brumback AC, Mathews GC, Benke TA, Delpire E, Jensen FE, Staley KJ (2005) NKCC1 transporter facilitates seizures in the developing brain. Nat Med 11:1205–1213.

Ebihara S, Shirato K, Harata N, Akaike N (1995) Gramicidin-perforated patch recording: GABA response in mammalian neurones with intact intracellular chloride. J Physiol (Lond) 484:77–86.

Fiumelli H, Cancedda L, Poo Mm (2005) Modulation of GABAergic transmission by activity via postsynaptic Ca^{2+}-dependent regulation of KCC2 function. Neuron 48:773–786.

Gao J, Mathias RT, Cohen IS, Baldo GJ (1995) Two functionally different Na/K pumps in cardiac ventricular myocytes. J Gen Physiol 106:995–1030.

Gasbjerg PK, Brahm J (1991) Kinetics of bicarbonate and chloride transport in human red cell membranes. J Gen Physiol 97:321–349.

Geck P, Pietrzyk C, Burckhardt BC, Pfeiffer B, Heinz E (1980) Electrically silent cotransport on Na^+, K^+ and Cl^- in Ehrlich cells. Biochim Biophys Acta 600:432–447.

Gillen CM, Brill S, Payne JA, Forbush III B (1996) Molecular cloning and functional expression of the K-Cl cotransporter from rabbit, rat, and human. A new member of the cation-chloride cotransporter family. J Biol Chem 271:16237–16244.

Ikeda M, Toyoda H, Yamada J, Okabe A, Sato K, Hotta Y, Fukuda A (2003) Differential development of cation-chloride cotransporters and Cl^- homeostasis contributes to differential GABAergic actions between developing rat visual cortex and dorsal lateral geniculate nucleus. Brain Res 984:149–159.

Jarolimek W, Lewen A, Misgeld U (1999) A furosemide-sensitive K^+-Cl^- cotransporter counteracts intracellular Cl^- accumulation and depletion in cultured rat midbrain neurons. J Neurosci 19:4695–4704.

Juhaszova M, Blaustein MP (1997) Na^+ pump low and high ouabain affinity alpha subunit isoforms are differently distributed in cells. Proc Natl Acad Sci USA 94:1800–1805.

Kahle KT, Rinehart J, los Heros P, Louvi A, Meade P, Vazquez N, Hebert SC, Gamba G, Gimenez I, Lifton RP (2005) WNK3 modulates transport of Cl^- in and out of cells: implications for control of cell volume and neuronal excitability. Proc Natl Acad Sci USA 102:16783–16788.

Khalilov I, Holmes GL, Ben Ari Y (2003) In vitro formation of a secondary epileptogenic mirror focus by interhippocampal propagation of seizures. Nat Neurosci 6:1079–1085.

Kyrozis A, Reichling DB (1995) Perforated-patch recording with gramicidin avoids artifactual changes in intracellular chloride concentration. J Neurosci Methods 57:27–35.

Lauf PK, Bauer J, Adragna NC, Fujise H, Zade-Oppen AM, Ryu KH, Delpire E (1992) Erythrocyte K^+-Cl^- cotransport: properties and regulation. Am J Physiol 263:C917–C932.

Läuger P (1987) Dynamics of ion transport systems in membranes. Physiol Rev 67:1296–1331.

Lu J, Karadsheh M, Delpire E (1999) Developmental regulation of the neuronal-specific isoform of K-Cl cotransporter KCC2 in postnatal rat brains. J Neurobiol 39:558–568.

Marty S, Wehrle R, Alvarez-Leefmans FJ, Gasnier B, Sotelo C (2002) Postnatal maturation of Na^+, K^+, 2Cl^- cotransporter expression and inhibitory synaptogenesis in the rat hippocampus: an immunocytochemical analysis. Eur J Neurosci 15:233–245.

McCarren M, Alger BE (1987) Sodium-potassium pump inhibitors increase neuronal excitability in the rat hippocampal slice: role of a Ca^{2+}-dependent conductance. J Neurophysiol 57:496–509.

McDougal DB, Osborn LA (1976) Post-tetanic hyperpolarization, sodium-potassium-activated adenosine triphosphatase and high energy phosphate levels in garfish olfactory nerve. J Physiol (Lond) 256:41–60.

Michaelis L, Menten M (1913) Die kinetik der invertinwirkung. Biochem Zeitschrift 49:333–369.

Morita K, David G, Barrett JN, Barrett EF (1993) Posttetanic hyperpolarization produced by electrogenic Na^+-K^+ pump in lizard axons impaled near their motor terminals. J Neurophysiol 70:1874–1884.

Parker D, Hill R, Grillner S (1996) Electrogenic pump and a Ca^{2+}- dependent K^+ conductance contribute to a posttetanic hyperpolarization in lamprey sensory neurons. J Neurophysiol 76:540–553.

Payne JA (1997) Functional characterization of the neuronal-specific K-Cl cotransporter: implications for $[K^+]_o$ regulation. Am J Physiol 273:C1516–C1525.

Ritchie JM, Straub RW (1957) The hyperpolarization which follows activity in mammalian non-medullated fibres. J Physiol (Lond) 136:80–97.

Rivera C, Voipio J, Payne JA, Ruusuvuori E, Lahtinen H, Lamsa K, Pirvola U, Saarma M, Kaila K (1999) The K^+/Cl^- co-transporter KCC2 renders GABA hyperpolarizing during neuronal maturation. Nature 397:251–255.

Rose CR, Ransom BR (1997) Regulation of intracellular sodium in cultured rat hippocampal neurones. J Physiol 499:573–587.

Rose CR, Kovalchuk Y, Eilers J, Konnerth A (1999) Two-photon Na^+ imaging in spines and fine dendrites of central neurons. Pflugers Arch 439:201–207.

Ross ST, Soltesz I (2001) Long-term plasticity in interneurons of the dentate gyrus. Proc Natl Acad Sci USA 98:8874–8879.

Russell JM (2000) Sodium-potassium-chloride cotransport. Physiol Rev 80:211–276.

Staley KJ, Mody I (1992) Shunting of excitatory input to dentate gyrus granule cells by a depolarizing $GABA_A$ receptor-mediated postsynaptic conductance. J Neurophysiol 68:197–212.

Staley KJ, Proctor WR (1999) Modulation of mammalian dendritic $GABA_A$ receptor function by the kinetics of Cl^- and HCO_3^-. J Physiol 519:693–712.

Staley KJ, Soldo BL, Proctor WR (1995) Ionic mechanisms of neuronal excitation by inhibitory $GABA_A$ receptors. Science 269:977–981.

Stein V, Hermans-Borgmeyer I, Jentsch TJ, Hubner CA (2004) Expression of the KCl cotransporter KCC2 parallels neuronal maturation and the emergence of low intracellular chloride. J Comp Neurol 468:57–64.

Sweadner KJ (1989) Isozymes of the Na^+/K^+-ATPase. Biochim Biophys Acta 988:185–220.

Talos DM, Fishman RE, Park H, Folkerth RD, Follett PL, Volpe JJ, Jensen FE (2006) Developmental regulation of alpha-amino-3-hydroxy-5-methyl-4-isoxazole-propionic acid receptor subunit expression in forebrain and relationship to regional susceptibility to hypoxic/ischemic injury. I. Rodent cerebral white matter and cortex. J Comp Neurol 497:42–60.

Tas PW, Massa PT, Kress HG, Koschel K (1987) Characterization of an $Na^+/K^+/Cl^-$ co-transport in primary cultures of rat astrocytes. Biochim Biophys Acta 903:411–416.

Therien AG, Blostein R (2000) Mechanisms of sodium pump regulation. Am J Physiol Cell Physiol 279:C541–C566.

Thompson SM, Prince DA (1986) Activation of electrogenic sodium pump in hippocampal CA1 neurons following glutamate-induced depolarization. J Neurophysiol 56:507–522.

Tyzio R, Ivanov A, Bernard C, Holmes GL, Ben Ari Y, Khazipov R (2003) Membrane potential of CA3 hippocampal pyramidal cells during postnatal development. J Neurophysiol 90:2964–2972.

van den Pol AN, Obrietan K, Chen G (1996) Excitatory actions of GABA after neuronal trauma. J Neurosci 16:4283–4292.

Vardi N, Zhang LL, Payne JA, Sterling P (2000) Evidence that different cation chloride cotransporters in retinal neurons allow opposite responses to GABA. J Neurosci 20:7657–7663.

Wagner S, Castel M, Gainer H, Yarom Y (1997) GABA in the mammalian suprachiasmatic nucleus and its role in diurnal rhythmicity. Nature 387:598–603.

Wang C, Shimizu-Okabe C, Watanabe K, Okabe A, Matsuzaki H, Ogawa T, Mori N, Fukuda A, Sato K (2002) Developmental changes in KCC1, KCC2, and NKCC1 mRNA expressions in the rat brain. Brain Res Dev Brain Res 139:59–66.

Wang C, Ohno K, Furukawa T, Ueki T, Ikeda M, Fukuda A, Sato K (2005) Differential expression of KCC2 accounts for the differential GABA responses between relay and intrinsic neurons in the early postnatal rat olfactory bulb. Eur J Neurosci 21:1449–1455.

Wang HY, Huang RC (2004) Diurnal modulation of the Na^+/K^+-ATPase and spontaneous firing in the rat retinorecipient clock neurons. J Neurophysiol 92:2295–2301.

Woodin MA, Ganguly K, Poo MM (2003) Coincident pre- and postsynaptic activity modifies GABAergic synapses by postsynaptic changes in Cl^- transporter activity. Neuron 39:807–820.

Yu XM, Salter MW (1998) Gain control of NMDA-receptor currents by intracellular sodium. Nature 396:469–474.